

Purcell effect in two-dimensional photonic crystal slabs with triangular latticeSergey A. Dyakov ¹, Ilya M. Fradkin,^{1,2} Dmitry V. Yurasov ³, Vladimir A. Zinovyev ⁴,
Sergei G. Tikhodeev ^{5,6} and Nikolay A. Gippius¹¹*Skolkovo Institute of Science and Technology, Bolshoy Boulevard 30, str. 1, Moscow 143025, Russia*²*Moscow Institute of Physics and Technology, Institutskiy pereulok 9, Moscow Region 141701, Russia*³*Institute for Physics of Microstructures RAS, GSP-105, Nizhny Novgorod 603950, Russia*⁴*Rzhanov Institute of Semiconductor Physics, SB RAS, Novosibirsk 630090, Russia*⁵*Lomonosov Moscow State University, Leninskie Gory, GSP-1, Moscow 119991, Russia*⁶*A.M. Prokhorov General Physics Institute, Vavilova st. 38, Moscow 117942, Russia*

(Received 22 February 2023; revised 22 September 2023; accepted 25 September 2023; published 13 October 2023)

We present the results of theoretical studies of the Purcell effect in infinite photonic crystal slabs without defects or cavities. First, we describe a theoretical model for calculating total and external Purcell factors in two-dimensional photonic crystal slabs in terms of dipole's emissivity to the near field and the far field. Then we apply this theory to silicon photonic crystal slabs with triangular lattice on silica substrate and study how the Purcell factor depends on the wavelength and the dipole's position. We show that by placing the dipoles in the hot spots of modes with the zero group velocity, one can greatly enhance the Purcell factor in comparison to a homogeneous silicon slab. We demonstrate that this effect is associated with Van Hove singularities. We also calculate partial contributions to the total Purcell factor from different energy dissipation channels.

DOI: [10.1103/PhysRevB.108.155416](https://doi.org/10.1103/PhysRevB.108.155416)**I. INTRODUCTION**

The Purcell effect is a concept in physics related to the interaction of electromagnetic fields with a material or substance. It is named after the American physicist Edward Purcell, and it is a measure of how effectively excited molecules or quantum dots placed in a nonhomogeneous dielectric environment can recombine with radiation of photons. The probability of spontaneous emission of an emitter per unit time is determined by the local density of optical states, which can be changed by placing the emitter in an optical cavity. The ratio of the radiative decay rates, modified and unmodified by the cavity, is known as a Purcell factor. Thus, when the emitter is placed into a cavity, near an interface or into a photonic crystal, the Purcell factor changes due to interaction of the emitter's dipole moment with optical resonances. Therefore, one can greatly increase or decrease the Purcell factor by using photonic structure with proper geometry.

High values of the Purcell factor can be obtained, for example, in plasmonic nanoantennas [1–8], in metal-dielectric metamaterials [9,10] or in three-dimensional dielectric microcavities such as microspheres and microtoroids [11–15], where the local field enhancement is strong. However, there is a way of achieving high Purcell factor in structures without cavities. It is well known that in infinite chains of all-dielectric particles, the theoretical Purcell factor diverges at frequencies corresponding to band edges, where the group velocity tends to zero. Such points are called Van Hove singularities; they were originally described for crystalline lattices in solids [16]. In reality, the divergence never occurs due to a finite number of periods of the photonic crystal lattice, geometrical imperfections, and radiative losses. Nevertheless, the high Purcell factor was experimentally achieved in finite chains of

all-dielectric nanoparticles supporting multipolar Mie resonances [17–19]. In Ref. [20] it was demonstrated that high Purcell factor values can also be reached due to interference between the band-edge modes and a standing mode supported by the same array of dielectric particles.

Despite the attractiveness of one-dimensional chains of nanoparticles, quantum emitters are often placed into two-dimensional photonic crystal slabs [21–32]. The latter provide a great variety of photonic resonances, which properties can be controlled by choosing appropriate surface patterns. In contrast to one-dimensional periodic waveguides, in two-dimensional photonic crystal slabs, the Purcell factor does not diverge on the modes with quadratic dispersion. Because of this, photonic crystal slabs with modified lattice attract interest of researchers since they can provide modes with flatter dispersion. One of the examples of such structures is doubly-periodic gratings [33], while an extreme case of structures with flat dispersion modes is photonic crystal cavities and waveguides. Thus, in the literature, theoretical and experimental studies of spontaneous emission rate of emitters have been carried out in photonic crystal slabs with cavities and waveguides [34–38]. Owing to the small mode volume of a single localized mode or a set of closely spaced modes that have frequencies within the gap, the Purcell factor in such structures can be quite large. Due to the small physical volume of the resonator, the number of emitters for which the Purcell factor reaches large values is also small. In this regard, it is of great interest to study the Purcell effect for dipoles located in a photonic crystal slab without cavities, despite that the Purcell factor in them does not diverge. An advantage of such structures from the experimental viewpoint is that there is no need for measuring the photoluminescence signal from very small surface area or to have a technology

for precise positioning of emitters, because emitters located in the same position in different unit cells will have the same Purcell factor. Thus, almost the entire area of the fabricated metasurface can be used, in contrast to photonic crystals with a microcavity.

In this work, we consider the Purcell effect in infinite photonic crystal slabs without cavities and demonstrate that the Purcell factor in them can be greatly enhanced on flat-band modes in comparison to homogeneous slabs. In the first part of the manuscript, we present the theoretical background for calculation of the Purcell factor in two-dimensional photonic crystal slabs. In the second part, we apply this theory for electric dipoles located in two types of photonic crystal slabs, comprising (i) air holes in silicon and (ii) silicon rods in the air.

II. THEORETICAL BACKGROUND

We define the Purcell factor as a ratio of the radiation rates modified and unmodified by the cavity:

$$F_p = \frac{\Gamma_r^{\text{cav}}}{\Gamma_r}. \quad (1)$$

In order to utilize formula (1) for calculation of the Purcell factor, we will use the result of the semiclassical theory of radiation, which states that the quantum mechanical rate of radiative decay is proportional to the total power dissipated by classical dipole emitters (see Appendix A for details):

$$\Gamma_r = \frac{P}{\hbar\omega}, \quad (2)$$

where ω is the frequency of electromagnetic oscillations. This ratio leads us to an alternative formula for the Purcell factor which is very important from the viewpoint of optical simulations:

$$F_p(\omega) = \frac{P^{\text{cav}}(\omega)}{P(\omega)}, \quad (3)$$

where $P^{\text{cav}}(\omega)$ is the total power dissipated by dipole emitters in an inhomogeneous dielectric medium:

$$P^{\text{cav}}(\omega) = \iint \vec{S}(\omega) d\vec{A}, \quad (4)$$

where \vec{S} is the Poynting vector, $d\vec{A}$ is the surface element, and $P(\omega)$ is the total power that the same dipole emitters would dissipate if they were in a dielectric that is uniform and infinite in all three dimensions with a refractive index of n :

$$P(\omega) = \frac{|\vec{j}_0|^2 \omega^2 n}{3c^3}, \quad (5)$$

where c is the speed of light and \vec{j}_0 is the amplitude of current's oscillation. Integration in formula (4) over a closed surface is carried out near the dipole. If n is taken as 1, then formula (1) will describe the increase in the rate of spontaneous emission of dipoles relative to the same dipoles in vacuum. However, since quantum dots or dye molecules in real structures are located in a certain matrix, chemical properties of which often determine the very ability of emitters to radiate, sometimes it is convenient to consider just such a host matrix in formula (5) as a dielectric. In this case, the

Purcell factor will be determined by the presence of boundaries with other substances of this host matrix. In the above paradigm, dipole's emission for the most arbitrary systems can be calculated in terms of a local density of optical states using various difference methods such as finite difference time domain [39,40]. Below we present semianalytical theory focusing on layered systems with periodic spatial modulation of dielectric permittivity.

In layered systems, integration over a closed surface in formula (4) can be replaced by finding the algebraic sum of the powers emitted by the dipole vertically upward and downward:

$$P^{\text{cav}} = \iint \vec{S} d\vec{A} = P^+ + P^-, \quad (6)$$

where the powers P^\pm are calculated as integrals of the z -components of the Poynting vector in the planes $z = z_0 \pm 0$, taken at an infinitely small distance above and below the dipole located at coordinate z_0 :

$$P^\pm(\omega) \equiv P(z_0 \pm 0) = \iint_{-\infty}^{+\infty} S_z(\omega, \vec{\rho}, z_0 \pm 0) d^2 \vec{\rho}, \quad (7)$$

where $\vec{\rho} \equiv \{x, y\}$. In two-dimensionally periodic layers, integration over the coordinate space can be conveniently replaced with integration in the momentum space over the first Brillouin zone (see Appendix B for the proof of this fact). Thus, the resulting formula for calculating the total Purcell factor takes the form:

$$F_p^{\text{tot}}(\omega) = \frac{3c^3}{|j_0|^2 \omega^2 n} \iint_{\text{FBZ}} [\tilde{S}_z^+(\omega, \vec{q}) + \tilde{S}_z^-(\omega, \vec{q})] \frac{d^2 \vec{q}}{(2\pi)^2}, \quad (8)$$

where $\tilde{S}_z^\pm(\omega, \vec{q}) \equiv S_z(\omega, \vec{q}, z_0 \pm 0)$ is the z -projection of the Poynting vector calculated in the momentum space using the Fourier modal method [41,42] taking into account all Fourier harmonics [see Eq. (B5)], and $\vec{q} \equiv \{k_x, k_y\}$ is the in-plane wave vector inside the first Brillouin zone. In homogeneous layers, the first Brillouin zone is infinite, and the integration is performed over the entire momentum space:

$$F_p^{\text{tot}}(\omega) = \frac{3c^3}{|j_0|^2 \omega^2 n} \iint_{-\infty}^{+\infty} [\tilde{S}_z^+(\omega, \vec{q}) + \tilde{S}_z^-(\omega, \vec{q})] \frac{d^2 \vec{q}}{(2\pi)^2}. \quad (9)$$

Components of the Poynting vector S_z of oscillating dipoles depend on the dipole orientation and its positions within the structure and can be found by the Fourier modal method in the scattering matrix form (see Appendix B and Refs. [3,41–44] for details). In what follows, the integrand in formulas (8) and (9) will be referred to as a *near-field emissivity* of the dipole. It should be noted that in the framework of classical electrodynamics, the total Purcell factor and the near-field emissivity for point-dipoles can be calculated only in non-absorptive media (see Appendix C for details).

It is obvious that a part of the power emitted by the dipole is able to outcouple to the upper and (or) lower semi-infinite media. Therefore, if in the integrands in formulas (8) and (9) we take the Poynting vectors calculated in the planes located at an infinitely small distance above and below the layered structure, then as a result of integration we get an external

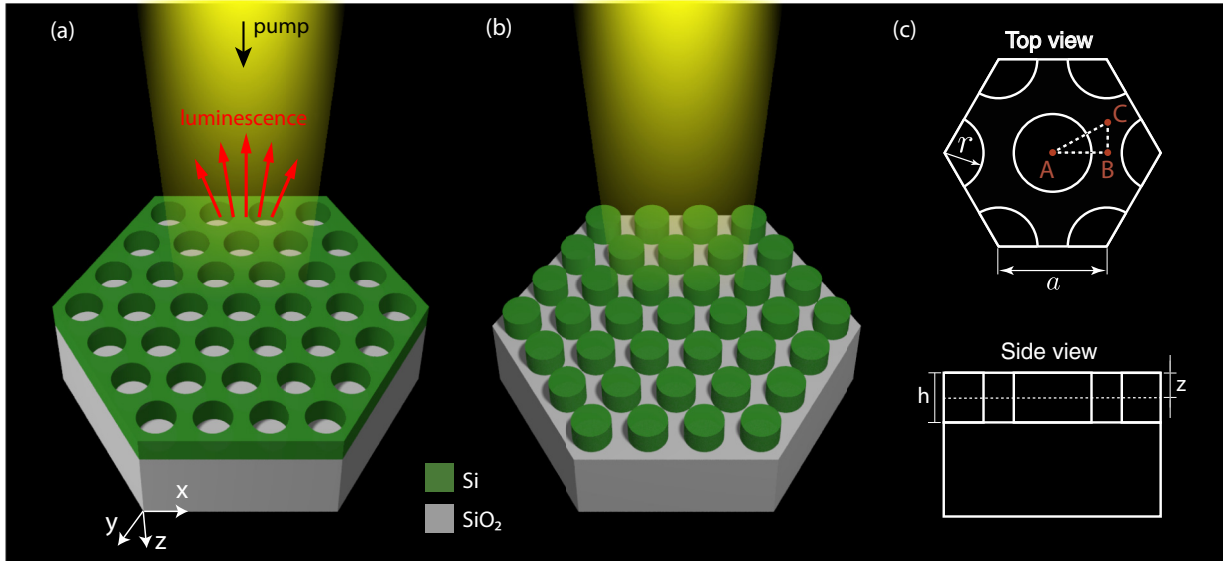


FIG. 1. Schematics of (a) an “inverse” and (b) “direct” photonic crystal waveguides, consisting of a z -uniform periodic air-silicon layer on a SiO_2 substrate, infinite in the xy plane. (c) Top view and side view of the waveguides along with the high-symmetry points on the photonic crystal unit cell. Photonic crystal slabs are characterized by the period a , thickness h , radius of cylinders r and the dipole position z .

part of the Purcell factor:

$$F_p^{\text{ext}}(\omega) = \frac{3c^3}{|j_0|^2 \omega^2 n} \iint_{\text{FBZ}} [\widehat{S}_z^+(\omega, \vec{q}) + \widehat{S}_z^-(\omega, \vec{q})] \frac{d^2 \vec{q}}{(2\pi)^2}, \quad (10)$$

where

$$\begin{aligned} \widehat{S}_z^-(\omega, \vec{q}) &\equiv S_z(\omega, \vec{q}, 0 - 0), \\ \widehat{S}_z^+(\omega, \vec{q}) &\equiv S_z(\omega, \vec{q}, h + 0), \end{aligned} \quad (11)$$

and h is the thickness of the entire structure between substrate and superstrate. By definition, the external Purcell factor is responsible for that part of enhancement (or attenuation) of spontaneous emission rate, which is determined by the power outcoupled to the far field.

The corresponding integrand in Eq. (10) is called a *far-field emissivity* in what follows. As in the case of the total Purcell factor for a periodic structure, the integration is performed over the first Brillouin zone regardless of the location of the light cones of the upper and lower semi-infinite media, and the \widehat{S}_z^\pm values are calculated by summation over all diffraction channels. It should be noted that according to formula (10) the external Purcell factor includes not only the power propagating in the substrate or superstrate but also the power which is absorbed in them. See Appendix C for the details of calculation of the far-field emissivity.

In the literature, a similar approach for calculation of the Purcell factor by integration of the dipole’s emissivity over the first Brillouin zone is referred to as the array scanning method [45,46]. An advantage of this method is that it represents a rigorous procedure independent on resonant properties of the photonic crystal slab. This is in contrast to the approach based on the representation of the local density of optical states as a sum of contributions of known *a priori* resonances of the system [40,47]. Using a resonant approximation for the scattering matrix [48–51] one can bridge the gap between

Eq. (9) and a commonly used resonance-based formula for the Purcell factor containing terms inversely proportional to the group velocity.

The possibility of calculating the Purcell factor in photonic structures makes it possible to predict the lifetime and intensity of photoluminescence of quantum dots located in them, as well as to evaluate their internal and external quantum efficiency [4,52–54].

III. THEORETICAL RESULTS

To obtain high values of the Purcell factor in photonic crystal slabs, we should place the electric dipoles into the hot spot of the eigenmode with zero group velocity; the scalar product of the dipole moment and the electric field in the eigenmode must not be zero. A great variety of available patterns and electric field profiles in two-dimensional metasurfaces makes it possible to find appropriate geometry for any dipole moment in a wide range of photon energies. In this work, we focus on x -, y -, and z -oriented electric dipoles located in two types of the photonic crystal slab: (i) an inverse one comprising air pores in silicon layer and (ii) a direct one comprising silicon rods in air (see Fig. 1). Both photonic crystal slabs have a triangular lattice and lie on the silica substrate. The choice of infinite “silica substrate” is an easy way to carry out the calculations. Nevertheless, it reflects the situation rather well because in reality the silicon-on-insulator substrates with a thick oxide layer ($\sim 3 \mu\text{m}$) are often used for fabrication of Si photonic structures. We denote the photonic crystal slab thickness as h , the period as a , and the radius of pores or rods as r . We place the electric dipole in points A, B, and C in the middle of the silicon layer as shown in Fig. 1.

Without loss of generality, we design the geometry of the photonic crystal slabs in such a way that at the photon energy of $\hbar\omega = 800 \text{ meV}$, the appropriate orientation of electric field and the zero group velocity of the band-edge mode will be demonstrated for the inverse photonic crystal slab; while the

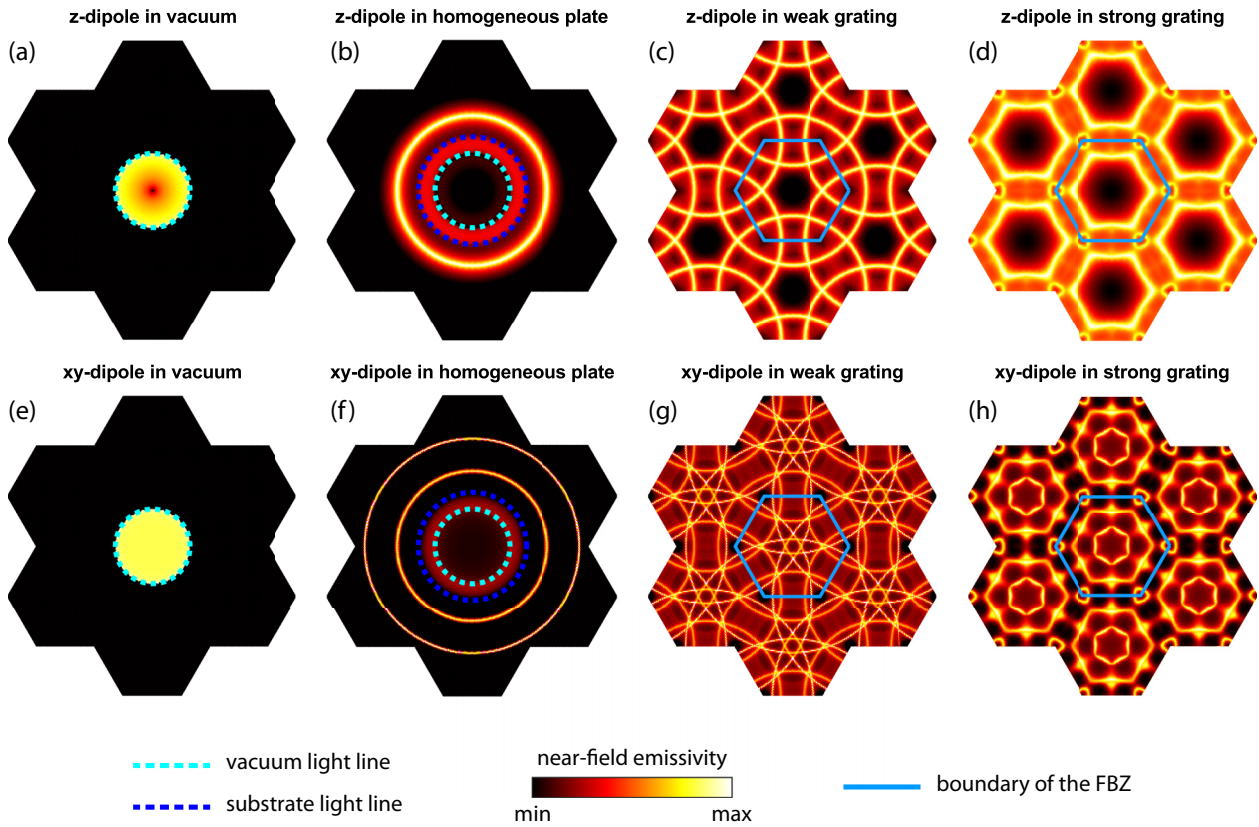


FIG. 2. In-plane wave-vector dependence of the near-field emissivity of horizontal dipoles (e)–(h) and vertical dipole (a)–(d), located in vacuum (a), (e), homogeneous silicon layer on SiO_2 substrate (b), (f), weak photonic crystal lattice (c), (g), strong photonic crystal lattice (d), (h). Calculations are made at $\hbar\omega = 850$ meV for the inverse photonic crystal slab with $h = 218$ nm, $a = 625$ nm, $r = 0.25a$. In (b), (f) the blue dashed line shows the light cone of the silica and the light blue dashed line indicates the light cone of the vacuum. (c), (d), (g), (h) show the boundary of the first Brillouin zone with white and black lines. The dipoles are located on the plane $z = 80$ nm. The color scale is logarithmic, shown in the inset below. The color scales in all parts are different. Dielectric constant of the pore substance of the weak lattice $\epsilon_{\text{pores}} = 1.001\epsilon_{\text{Si}}$.

same effect but on another guided resonance mode (not at the end of the first Brillouin zone) will be shown for the direct photonic crystal slab. The corresponding geometrical parameters of the inverse photonic crystal slab are the following: period $a = 445$ nm, pores' radius $r = 0.405a$, and slab thickness $h = 230$ nm. For the direct photonic crystal slab, the parameters are: period $a = 555$ nm, pores' radius $r = 0.4025a$, and slab thickness $h = 285$ nm. In calculations by the Fourier modal method (FMM) we use 85 Fourier harmonics [55].

Before calculation of the Purcell factor, let us first consider the dependence of the near-field emissivity of dipoles on the horizontal projection of the wave vector, $f(k_x, k_y)$. For vertical (z -oriented) dipoles and horizontal (average of x - and y -oriented) dipoles in vacuum, the near-field emissivity looks as shown in Figs. 2(a) and 2(e): outside the light cone this function is equal to 0, while inside the light cone it has z -axial symmetry. For the dipoles located in a homogeneous silicon layer without pores, the function $f(k_x, k_y)$ is more complicated, since the dipoles can radiate not only into the propagating modes of the upper and lower semi-infinite media, but also into the waveguide modes lying below the light cones of these media. Such waveguide modes in Figs. 2(b) and 2(f) are visible as rings centered at the origin ($k_x = k_y = 0$).

The functions $f(\vec{q})$ shown in Figs. 2(a), 2(b), 2(e), 2(f) have axial symmetry, therefore the double integral in the formula (9) can be replaced with a single one, thereby the time of numerical integration can be greatly reduced:

$$F_p(\omega) = \frac{3c^3}{|j_0|^2\omega^2n} \iint_{-\infty}^{+\infty} f(\vec{q})d^2\vec{q} = \quad (12)$$

$$\frac{3c^3}{|j_0|^2\omega^2n} \int_0^\infty f(k_x, 0)k_x dk_x \quad (13)$$

Let us now consider the inverse photonic crystal slab and assume that the emitting dipole is located at point A in the unit cell (see Fig. 1), the most symmetrically located point between the pores. Let us start with a *weak* photonic crystal lattice, i.e., a structure similar to that shown in Fig. 1, but with pores filled with a substance with a dielectric constant slightly different from the dielectric constant of silicon ($\epsilon_{\text{pores}} = 1.001\epsilon_{\text{Si}}$). The weak contrast of such a grating almost does not change the dispersion of the waveguide modes, but diffraction on the periodicity folds the waveguide modes into the first Brillouin zone, as shown in Figs. 2(c) and 2(g). Integration performed inside the first Brillouin zone over the near-field emissivity in a weak grating will give a value of the total Purcell factor

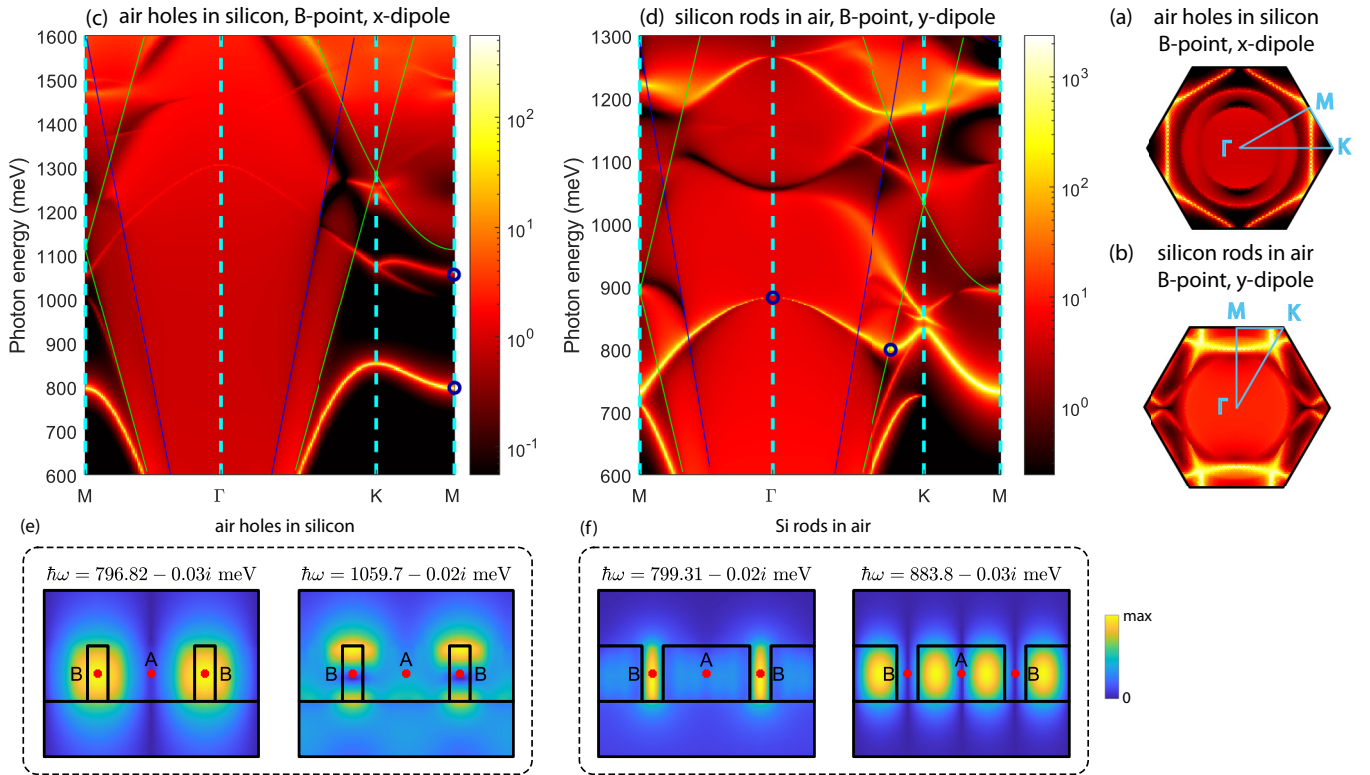


FIG. 3. (a) and (b) Near-field emissivity in the first Brillouin zone calculated at the photon energy of $\hbar\omega = 800$ meV for B point and x dipole in the inverse photonic crystal slab and B point and y dipole in the direct photonic crystal slab. (c) and (d) Photon energy and in-plane wave-vector dependence of the near-field emissivity of the inverse and direct photonic crystal slabs. High-symmetry points of the first Brillouin zone Γ , M, and K are defined in (a) and (b). Blue and green lines in (c) and (d) denote light-lines of air and silica, correspondingly. (e) and (f) Electric field intensity profiles in some of the eigenmodes. In (e) the fields are calculated for M point, while in (f) for $(k_x, k_y) = (0.704k_0, 1.272k_0)$ (left part) and for Γ point (right part). Blue circles in (c) and (d) denote eigenmodes for which the fields in (e) and (f) are plotted.

very close to the value in the original nonperiodic waveguide. Finally, in a *strong* photonic crystal lattice, where the etched pores are filled with air, the waveguide modes folded into the first Brillouin zone hybridize, which results in a rather complex profile of the C_6 -symmetric function $f(k_x, k_y)$ shown in Figs. 2(d) and 2(h) for horizontal and vertical dipoles. Note that for dipoles that are located not at high symmetric point A, the function $f(\vec{q})$ will no longer have the symmetry C_6 . Integration of such a profile with a number of harmonics sufficient for FMM convergence can take a long time in the case of high-Q resonances. To avoid this, as mentioned in Appendix C, we add a small imaginary part to the dielectric constant of the substrate ($0.001i$) for calculation of the total Purcell factor and to the dielectric permittivity of silicon for calculation of the external Purcell factor ($0.05i$) [56]. Therefore, Fig. 2 describes the genesis of the near-field emissivity starting from the homogeneous slab through the weak photonic crystal to the strong photonic crystal. It bridges the gap between a well-known donutlike angular emission diagram of an oscillating dipole in free space and an emissivity profile inside the first Brillouin zone for the same dipole in a photonic crystal slab.

Next, we calculate the photon energy and wave-vector dependences of the near-field emissivity for the x dipole at point B of the inverse photonic crystal slab and for the y dipole at point B of the direct photonic crystal slab (Figs. 3(c) and 3(d)). The resulting spectra of the total Purcell factor

are shown in Figs. 4(d) and 4(f) by the red line. One can see from Fig. 3 that in both cases there are several modes with the zero group velocity, while the peak values of the Purcell factor are achieved only at the photon energy of $\hbar\omega = 800$ meV (4). This is because only some of the modes have electric field distributions with local maxima at dipoles' positions [see Figs. 3(e) and 3(f) for field distribution in some of the modes). Thus, the enhancement of Purcell factor in our structures is indeed associated with Van Hove singularities. See Appendix D for the analytical expressions for the local density of optical states containing group velocity of the resonances.

Depending on the photon energy and the in-plane wave vector, the electric dipole can dissipate its energy via one of several channels [see sketch in Fig. 4(a)]. For example, if the point (ω, \vec{q}) in Figs. 3(c) and 3(d) is below the substrate light line and the substrate is lossless, then the emitted light is coupled only to the guided modes. However, if the point (ω, \vec{q}) is between the substrate and air light cones, then the emitted light can outcouple to the substrate far-field via the main or diffraction channels; in the case of lossless substrate, it can also couple to the guided modes. Finally, for the points (ω, \vec{q}) above the air light line, all mentioned energy dissipation channels are available. As it has been stated in the previous section, in the case of a lossy substrate, the wave will eventually be absorbed in it, although this process may occur via coupling to guided modes.

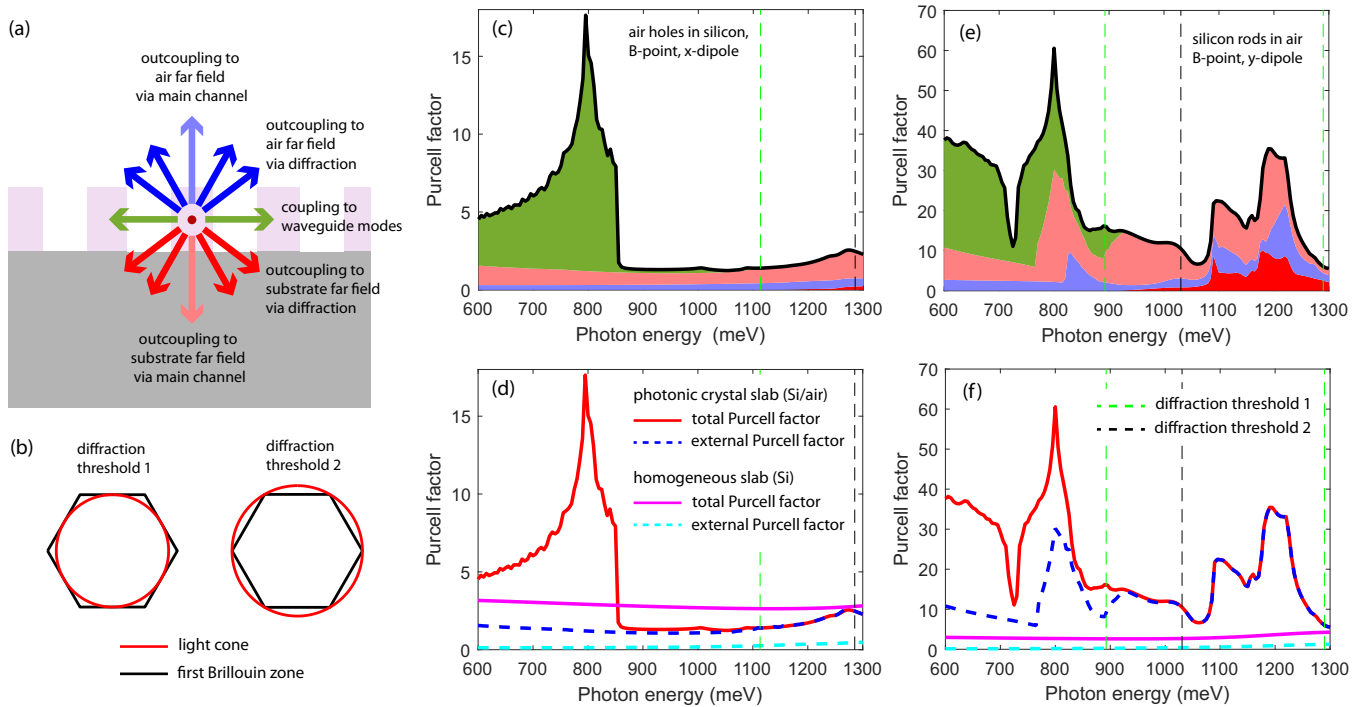


FIG. 4. (a) The sketch showing channels of energy dissipation of an emitting dipole located in a photonic crystals slab. (b) The first Brillouin zone of the triangular photonic crystal lattice superimposed on the light cones with photon energies corresponding to two diffraction thresholds. (c) The spectrum of the total Purcell factor (black line) and its partial contributions from different energy dissipation channels (colored areas) calculated for the inverted photonic crystal slab. Definition of colors is shown by arrows in (a). (d) The spectra of the total Purcell factor (red solid line) and external Purcell factor (blue dashed line) of the inverted photonic crystal slab in comparison to those of the homogeneous Si slab on silica substrate. (e) and (f) the same as (c) and (d) but calculated for the direct photonic crystal slab. In (c)–(f) vertical green and black dashed lines denote energies of the upper and lower diffraction thresholds. Parameters of the inverted photonic crystal slab: $a = 445$ nm, $h = 230$ nm, $r = 0.405a$, $z = h/2$. Parameters of the direct photonic crystal slab: $a = 555$ nm, $h = 285$ nm, $r = 0.4025a$, $z = h/2$.

Figures 4(c) and 4(e) plots the spectral dependences of the total Purcell factor along with the resulting spectra of partial contributions from all energy dissipation channels. One can see from Fig. 4(c) that for the inverse photonic crystal slab, the increase of the total Purcell factor in range 600–860 meV is attributed only to the enhanced coupling of the emitted wave to the waveguide modes. This is because the corresponding waveguide mode lies entirely below the substrate light line [see Fig. 3(c)]. Note that this mode gives rise to the $\hbar\omega = 800$ meV peak in the Purcell factor spectrum, both for x and y dipoles located at B and C points [56]. However, the peak value of the Purcell factor exceeds 10 only in the case of x dipole located at point B. This fact is attributed to specific orientation of electric vector in the mode at this photon energy. For the direct photonic crystal slab, the situation is different. The mode with a zero group velocity intersects the air and substrate light cones at $\hbar\omega = 800$ meV [Fig. 3(d)], which results in the increase of coupling of the emitted light not only to the waveguide modes but also to the air and substrate via the main channels. The local maxima of the Purcell factor spectrum $\hbar\omega = 800$ meV in the case of x and y dipoles located at A, B, and C points are also present [56], but their peak values are not so high as for the x dipole at B point, which is also explained by the direction of the electric vector in the mode.

Another important feature in the spectra of different energy dissipation channels, is that there is a photon energy range

where with the increase of the photon energy, the coupling to waveguide modes decreases to zero, while the outcoupling to substrate via diffraction starts to increase [see green and red areas in Figs. 4(c) and 4(d)]. This energy range is bounded by two diffraction thresholds. An upper diffraction threshold corresponds to the case when the first Brillouin zone of the photonic crystal lattice is fully inside the substrate light cone [Fig. 4(b)]. It means that for $\hbar\omega > E_{\text{th}}^{(2)}$, a wave emitted with any wavevector will eventually diffract to the substrate. There is also a lower diffraction threshold, when the light cone is tangent to the first Brillouin zone. For $E_{\text{th}}^{(\text{upper})} > \hbar\omega > E_{\text{th}}^{(\text{lower})}$, diffraction to the substrate occurs too, but not for all points inside the first Brillouin zone. For a triangular photonic crystal lattice of period a , the photon energies of the upper and lower diffraction thresholds are

$$E_{\text{th}}^{(\text{upper})} = \frac{4\pi}{3n} \frac{\hbar c}{a}, \quad E_{\text{th}}^{(\text{lower})} = \frac{2\pi\sqrt{3}}{3n} \frac{\hbar c}{a}, \quad (14)$$

where n is the refractive index of the substrate.

The sum of partial contributions of energy dissipation channels to the air and substrate corresponds to the external Purcell factor. The total and external Purcell factors of the direct and inverse photonic crystal slabs are shown in Figs. 4(d) and 4(f) in comparison with those of the homogeneous silicon slab of the same thickness. From these figures one can see in the case of the homogeneous silicon slab, the total Purcell

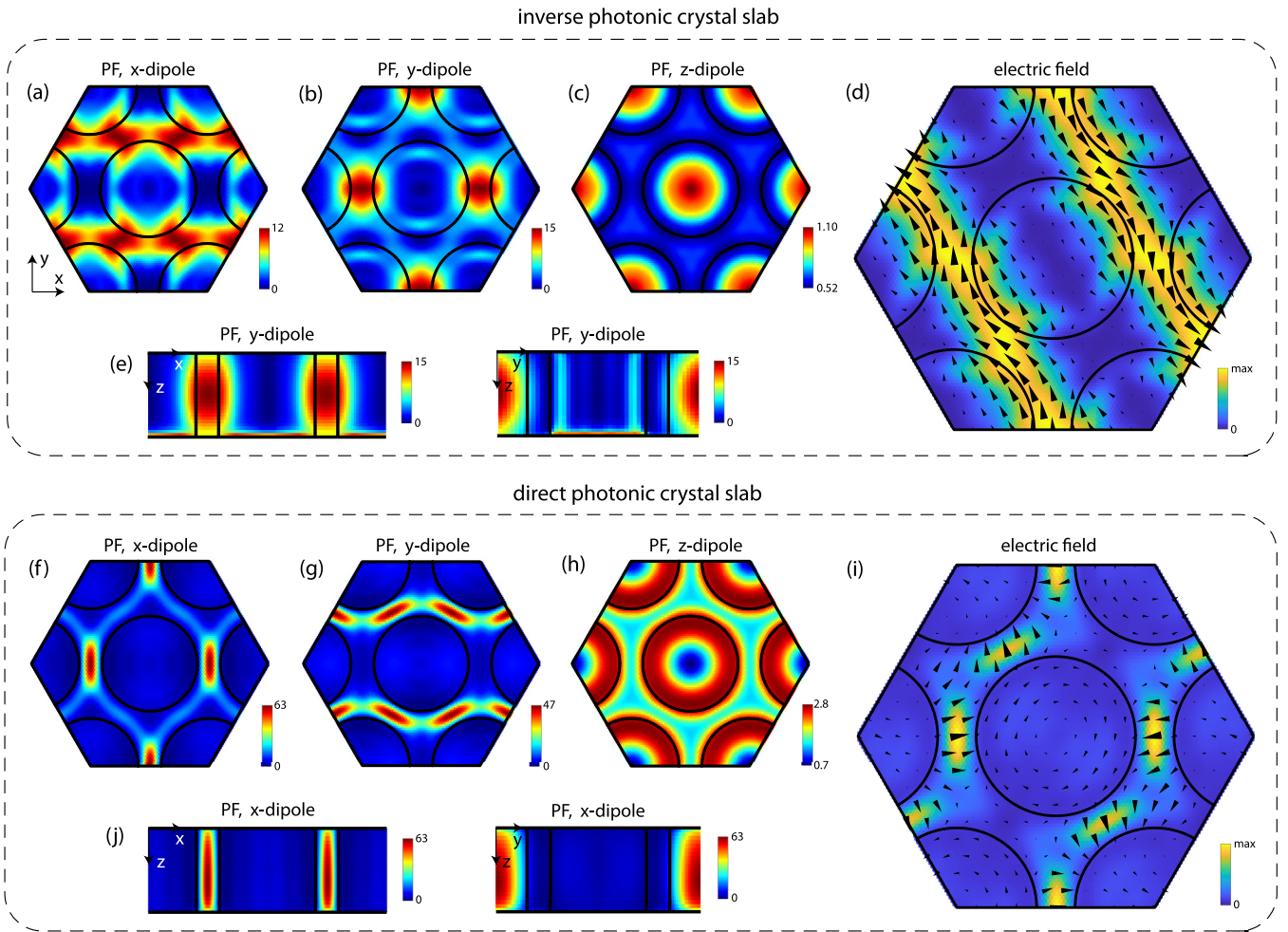


FIG. 5. Spatial distributions of the total Purcell factor of x , y , z polarized dipoles located on the plane $z = h/2$ calculated for the inverse [(a), (b), (c), (e)] and direct [(f), (g), (h), (j)] photonic crystal slabs at the photon energy $\hbar\omega = 800$ meV in the xy , xz , and yz cross sections passing through the center of the cell. (d) and (i) Electric field distribution in the eigenmodes ($\hbar\omega_{\text{em}}^{\text{inverse}} = 797 - 0.03i$ meV, $\hbar\omega_{\text{em}}^{\text{direct}} = 799 - 0.02i$ meV) of the inverse and direct photonic crystal slabs. Color denotes intensity, arrows show electric vector. Parameters of the inverted photonic crystal slab: $a = 445$ nm, $h = 230$ nm, $r = 0.405a$, $z = h/2$. Parameters of the direct photonic crystal slab: $a = 555$ nm, $h = 285$ nm, $r = 0.4025a$, $z = h/2$.

factor greatly exceeds the external Purcell factor. This effect is well known and is explained by the fact that radiation from an homogeneous layer outcouples to the far field only from a small solid angle. The structure periodicity gives rise to the external Purcell factor due to the diffraction coupling between the near and far fields. At $\hbar\omega > E_{\text{th}}^{\text{(upper)}}$, the external Purcell becomes equal to the total Purcell factor, as it has been discussed above. As for the total Purcell factor, in the photonic crystal slab it can be larger or smaller than in the homogeneous slab depending on the photon energy and the structure.

From Fig. 4 an important conclusion can be made that the photonic crystal lattice is especially effective in terms of increasing the external Purcell factor, since it connects the near and far fields due to diffraction. At the same time, to increase the total Purcell factor, a photonic crystal lattice can also be used, but for this, the cell must be designed in such a way that (a) it had the flattest possible dispersion curve at the photon energy of interest; (b) dipoles should be

located in the modes hot spots; (c) orientations of the dipole's moment and electric vector in the eigenmode should match. Low-dispersion waveguide modes can be obtained using, for example, superlattices with a double period.

Finally, the spatial maps of the total Purcell factor for x , y , z dipoles inside the photonic crystal cell are shown in Fig. 5 for the photon energy $\hbar\omega = 800$ meV along with the profile of electric field in the eigenmode. One can see that the presented maps manifest hot spots where the dipole's orientation matches that of the electric field. In these hot spots, the Purcell factor reaches a value of $F_p = 63$ for the x dipole at the B point in the direct photonic crystal slab and a value of $F_p = 15$ for the y dipole at the B point in the inverse photonic crystal slab. Also, in Figs. 5(e) and 5(j) one can see that the Purcell factor is distributed over the z direction quite uniformly. The nonuniformity of the spatial distribution of the Purcell factor is one of the reasons for non-mono-exponentiality of the photoluminescence decay profile observed in experiments.

IV. CONCLUSION

In conclusion, we have presented a model for theoretical description of the Purcell effect in photonic crystal slabs. Using this theoretical model, we have calculated and analyzed the total and external Purcell factors for x , y , and z dipoles located in different points of silicon photonic crystal slabs with triangular lattice. We have demonstrated that at the photon energies corresponding to zero group velocities of waveguide modes, the Purcell factor of dipoles located at the modes' hot spots, can be greatly increased in comparison to the homogeneous silicon waveguide. We have found geometrical parameters of the photonic crystal slab to obtain high values of the Purcell factor at the photon energy of 800 meV. We also have shown the spectra of different energy dissipation channels contributing to the total Purcell factor and have demonstrated that at photon energies larger than the upper diffraction threshold, the total and external Purcell factor are equal. Finally, we have presented the spatial maps of the total Purcell factor within the cell of the photonic crystal lattice.

ACKNOWLEDGMENTS

S.A.D. and D.V.Y. contributed to the conceptualization of the article, FMM calculations, analysis of the results, and manuscript preparation (Secs. I, III, Appendix A, and Appendix C). I.M.F., S.G.T., and N.A.G. contributed to the development of the theoretical basis for calculating the Purcell factor using Fourier Modal Method (Section II, Appendix B, and Appendix D). S.A.D. and D.V.Y. acknowledge the financial support provided by Russian Science Foundation (Grant No. 19-72-10011). I.M.F., S.G.T., and N.A.G. acknowledge the financial support from Russian Science Foundation (Grant No. 22-12-00351).

APPENDIX A: DIPOLE IN SEMICLASSICAL THEORY OF RADIATION

In order to utilize formula (1) for calculation of the Purcell factor, we will use the result of the semiclassical theory of radiation, which states that the quantum mechanical rate of radiative decay is proportional to the total power dissipated by classical dipole emitters. Let us show this by considering the classical model of a scattering dipole with energy E and total power flux P . The total energy stored in the dipole is proportional to the square of the amplitude of the dipole moment p [47]:

$$E = \alpha p^2, \quad (\text{A1})$$

where α is the proportionality coefficient. Here we assume that the dipole is *not infinitesimal*. This important assumption solves the problem of the diverging energy density of electric field near the dipole. The dissipated power of the dipole is also proportional to the square of the amplitude of the dipole moment:

$$P = \beta p^2, \quad (\text{A2})$$

where β is the proportionality coefficient. Since $\dot{E} = -P$, we get the following differential equation:

$$2\alpha \dot{p} = \beta p \quad (\text{A3})$$

with solution

$$p(t) = p_0 e^{-\frac{\beta}{2\alpha} t}. \quad (\text{A4})$$

Consequently, the energy and power flux decrease as

$$E(t) = \alpha p_0^2 e^{-\frac{\beta}{\alpha} t}, P(t) = \beta p_0^2 e^{-\frac{\beta}{\alpha} t}, \quad (\text{A5})$$

with the same decay constant Γ_r :

$$\Gamma = \frac{\beta}{\alpha} = \frac{P}{E}. \quad (\text{A6})$$

Replacing E with the energy of the emitted photon $\hbar\omega$, we obtain the required ratio between the power dissipated and the radiative decay rate:

$$\Gamma_r = \frac{P}{\hbar\omega}. \quad (\text{A7})$$

APPENDIX B: CALCULATION OF DIPOLE RADIATION IN MOMENTUM SPACE BY FOURIER MODAL METHOD

In order to prove that the total power emitted by a dipole can be represented as an integral over the momentum space, we start with an arbitrary (i.e., not necessarily periodic) slab. The electric and magnetic fields in such a slab can be expressed as an inverse Fourier transform:

$$\begin{aligned} \vec{E}(\vec{\rho}, z) &= \int \vec{E}(\vec{q}, z) e^{i\vec{q}\vec{\rho}} \frac{d^2\vec{q}}{(2\pi)^2}, \\ \vec{H}(\vec{\rho}, z) &= \int \vec{H}(\vec{q}, z) e^{i\vec{q}\vec{\rho}} \frac{d^2\vec{q}}{(2\pi)^2}, \end{aligned} \quad (\text{B1})$$

where $\vec{\rho} \equiv \{x, y\}$, $\vec{q} \equiv \{k_x, k_y\}$. An expression for time-average the total power flux through the horizontal plane $z = z_0$ reads

$$\begin{aligned} P &= \frac{c}{8\pi} \int \text{Re}[\vec{E}(\vec{\rho}) \times \vec{H}^*(\vec{\rho})]_z d^2\vec{\rho} \\ &= \frac{c}{8\pi} \int \frac{d^2\vec{q}}{(2\pi)^2} \frac{d^2\vec{q}'}{(2\pi)^2} \text{Re}[\vec{E}(\vec{q}) \times \vec{H}^*(\vec{q}')]_z \int d^2\vec{\rho} e^{i(\vec{q}-\vec{q}')\vec{\rho}} \\ &= \frac{c}{8\pi} \int \text{Re}[\vec{E}(\vec{q}) \times \vec{H}^*(\vec{q})]_z \frac{d^2\vec{q}}{(2\pi)^2}. \end{aligned} \quad (\text{B2})$$

In slabs with an arbitrary distribution of the refractive index and with a finite number of dipole sources, the integration in formula (B2) is rather complicated. However, in periodic slabs considered by the Fourier modal method, the situation is much simpler because of two facts. First, the fields are represented by a finite-size hypervector of the Floquet-Fourier components. Second, in the FMM, the infinite set of oscillating dipoles (currents) is considered. The corresponding hypervector of oscillating currents has the form

$$\mathbf{J}_{\alpha\gamma}(\vec{q}) = j_\alpha e^{-i\vec{\rho}_a(\vec{q} + \vec{g}_\gamma)}, \quad (\text{B3})$$

where j_α are the components of current in real space ($\alpha = x, y, z$), \vec{g}_γ is a vector in reciprocal space, representing γ -th harmonic ($\gamma = 1 \dots N_\gamma$, where N_γ is the number of Fourier harmonics). Therefore, the integration over the entire q space in formula (B2) can be replaced with the integration over the first Brillouin zone and summation over the entire set of

harmonics:

$$P(z) = \frac{c}{8\pi} \int_{\text{FBZ}} \sum_{\gamma=1}^{N_\gamma} \text{Re}[\tilde{\mathbf{E}}_\gamma(\vec{q}, z) \times \tilde{\mathbf{H}}_\gamma^*(\vec{q}, z)]_z \frac{d^2\vec{q}}{(2\pi)^2}. \quad (\text{B4})$$

The final expression for the total Purcell reads

$$F_p^{\text{tot}}(\omega) = \frac{3c^3}{|j_0|^2 \omega^2 n} \iint_{\text{FBZ}} [\tilde{\mathbf{S}}_z^+(\omega, \vec{q}) + \tilde{\mathbf{S}}_z^-(\omega, \vec{q})] \frac{d^2\vec{q}}{(2\pi)^2}, \quad (\text{B5})$$

where ‘‘FBZ’’ stands for the first Brillouin zone, n is the refractive index of the dielectric (for example, emitter’s host matrix or vacuum), relative to which the Purcell factor is calculated, and the z components of the Poynting vector are found as

$$\begin{aligned} \tilde{\mathbf{S}}_z^\pm(\omega, \vec{q}) = & \frac{c}{16\pi} \left[\sum_{\gamma=1}^{N_\gamma} (\mathbf{E}_{x\gamma}^*(\omega, \vec{q}, z_0 \pm 0) \cdot \mathbf{H}_{y\gamma}(\omega, \vec{q}, z_0 \pm 0)) + \sum_{\gamma=1}^{N_\gamma} (\mathbf{E}_{x\gamma}(\omega, \vec{q}, z_0 \pm 0) \cdot \mathbf{H}_{y\gamma}^*(\omega, \vec{q}, z_0 \pm 0)) \right. \\ & \left. - \sum_{\gamma=1}^{N_\gamma} (\mathbf{E}_{y\gamma}^*(\omega, \vec{q}, z_0 \pm 0) \cdot \mathbf{H}_{x\gamma}(\omega, \vec{q}, z_0 \pm 0)) - \sum_{\gamma=1}^{N_\gamma} (\mathbf{E}_{y\gamma}(\omega, \vec{q}, z_0 \pm 0) \cdot \mathbf{H}_{x\gamma}^*(\omega, \vec{q}, z_0 \pm 0)) \right]. \quad (\text{B6}) \end{aligned}$$

In formula (B6), $\mathbf{E}_{x\gamma, y\gamma}$ and $\mathbf{H}_{x\gamma, y\gamma}$ are the $N_\gamma \times 1$ hypervectors of electric and magnetic field radiated by oscillating currents. These hypervectors are found from the hypervectors of currents $\mathbf{J}_{\alpha\gamma}$ [3,43,57–60]:

$$\begin{bmatrix} \mathbf{E}_x \\ \mathbf{E}_y \\ \mathbf{H}_x \\ \mathbf{H}_y \end{bmatrix}_{z=z_0+0} = \mathbb{F} \begin{bmatrix} (\mathbb{I} - \mathbb{S}_{12}^u \mathbb{S}_{21}^d)^{-1} & -(\mathbb{I} - \mathbb{S}_{12}^u \mathbb{S}_{21}^d)^{-1} \mathbb{S}_{12}^u \\ \mathbb{S}_{21}^d (\mathbb{I} - \mathbb{S}_{12}^u \mathbb{S}_{21}^d)^{-1} & -\mathbb{S}_{21}^d (\mathbb{I} - \mathbb{S}_{12}^u \mathbb{S}_{21}^d)^{-1} \mathbb{S}_{12}^u \end{bmatrix} \mathbb{F}^{-1} \begin{bmatrix} +K_x \tilde{\epsilon}^{33} \mathbf{J}_z / k_0 \\ +K_y \tilde{\epsilon}^{33} \mathbf{J}_z / k_0 \\ +\mathbf{J}_y - \tilde{\epsilon}^{23} \tilde{\epsilon}^{33} \mathbf{J}_z \\ -\mathbf{J}_x + \tilde{\epsilon}^{13} \tilde{\epsilon}^{33} \mathbf{J}_z \end{bmatrix}, \quad (\text{B7})$$

$$\begin{bmatrix} \mathbf{E}_x \\ \mathbf{E}_y \\ \mathbf{H}_x \\ \mathbf{H}_y \end{bmatrix}_{z=z_0-0} = \mathbb{F} \begin{bmatrix} -\mathbb{S}_{12}^u (\mathbb{S}_{21}^d \mathbb{S}_{12}^u - \mathbb{I})^{-1} \mathbb{S}_{21}^d & \mathbb{S}_{12}^u (\mathbb{S}_{21}^d \mathbb{S}_{12}^u - \mathbb{I})^{-1} \\ -(\mathbb{S}_{21}^d \mathbb{S}_{12}^u - \mathbb{I})^{-1} \mathbb{S}_{21}^d & (\mathbb{S}_{21}^d \mathbb{S}_{12}^u - \mathbb{I})^{-1} \end{bmatrix} \mathbb{F}^{-1} \begin{bmatrix} +K_x \tilde{\epsilon}^{33} \mathbf{J}_z / k_0 \\ +K_y \tilde{\epsilon}^{33} \mathbf{J}_z / k_0 \\ +\mathbf{J}_y - \tilde{\epsilon}^{23} \tilde{\epsilon}^{33} \mathbf{J}_z \\ -\mathbf{J}_x + \tilde{\epsilon}^{13} \tilde{\epsilon}^{33} \mathbf{J}_z \end{bmatrix}, \quad (\text{B8})$$

where \mathbb{F} is the material matrix of the layer where the currents are located, indices ‘‘+’’ and ‘‘-’’ mean that corresponding quantities are taken below or above the plane $z = z_0$. In Eqs. (B7) and (B8) the upper and lower partial scattering matrices (\mathbb{S}^u and \mathbb{S}^d) are calculated at given ω , z and \vec{q} [3,41]. The matrix $\tilde{\epsilon}$ is the 3×3 block matrix with components that evolve from the Fourier transform of dielectric permittivity tensor (or its inverse) [61] calculated in accordance with Li’s factorization rules [62]; $K_{x,y}$ are the diagonal matrices of x - and y -components of photon quasimomentum vector of different diffraction orders; k_0 is the photon wave number in vacuum.

APPENDIX C: NOTES ON CALCULATION OF PURCELL FACTOR IN PHOTONIC CRYSTAL SLABS

It should be noted that the near-field emissivity diverges if a point dipole is located in absorbing material. This is due to the fact that the absorption of the electromagnetic field emitted by the point dipole inside a small sphere around this dipole tends to infinity as the radius of the sphere decreases to 0 (see, e.g., in Refs. [3,63]). To handle this problem, we must assume that either the emitter is not a point dipole, or that its host matrix is nonabsorbing. Despite the fact that the assumption that the emitter is not a point dipole that is closest to physical

reality, we will use the second approach. It means that we will solve Maxwell’s equations, in which the current density of the oscillating dipole appears in the form of a delta function, and the medium in which this current is located has a zero imaginary part of the dielectric permittivity. This approach to handling the problem of the diverging field of a dipole has its advantages. First, Maxwell’s equations with a current in the form of a delta function are solved quite simply, and the solution itself can be easily incorporated into many solvers, including the formalism of the FMM. Second, this approach avoids additional fitting parameters associated with the size and shape of the nonpoint dipole. Finally, if the concentration of emitters is low enough, ellipsometric studies of a substance with an emitter do indeed give a very small imaginary part of the permittivity, which can be neglected.

Let us make a number of important remarks concerning the calculation of Purcell factors in layered structures.

(1). According to the definitions given above, the following inequality always holds:

$$F_p^{\text{ext}} \leq F_p. \quad (\text{C1})$$

The external and total Purcell factors are equal in the following cases:

(a) Nonabsorbing (homogeneous or periodic) layers are located between two semi-infinite media, at least one of which is

absorbing; in such a structure, a wave emitted by a dipole will be absorbed with 100% probability in one of the semi-infinite media;

(b) The first Brillouin zone of a two-dimensional periodic structure, consisting of non-absorbing materials, is entirely located inside the light cone of at least one of two semi-infinite media; in this case, all eigenmodes of such a periodic structure are connected with the far field of this semi-infinite medium due to diffraction, which also provides a 100% probability for a wave to outcouple into the corresponding far field (this case will be considered in the next paragraph).

(2). A structure (homogeneous or periodic), consisting of nonabsorbing materials, located between two nonabsorbing semi-infinite media, can have its guided modes that are not connected with the far field. These modes would have an infinite Q factor. We can say that these modes appear as infinitely narrow peaks in the in-plane wave-vector dependence of the near-field emissivity, which must be integrated to calculate the full Purcell factor. To integrate such a dependence, we introduce a small material absorption into the system, thereby setting the finite width of such waveguide modes. Since, as already mentioned, for the convergence of the integral, some vicinity of the dipole must be nonabsorbing, it is convenient to add a small imaginary part $\text{Im}\varepsilon$ to the permittivity of the substrate. When choosing the imaginary addition, it is necessary to find the tradeoff balance between the integration time (the larger $\text{Im}\varepsilon$ the faster integration) and the convergence of this procedure with respect to the parameter $\text{Im}\varepsilon$ (the smaller $\text{Im}\varepsilon$ the less the Purcell factor is affected by it). Note that when calculating the external Purcell factor, the indicated problem of infinitely narrow peaks, cannot arise by definition, since only the modes connected with the far field are involved in the external Purcell factor, thereby having a noninfinite Q factor. Nevertheless, sometimes the radiation bandwidths of the modes are too small for integration to be complete in a reasonable time. For this reason, and also according to Remark (1), when calculating the external Purcell factor, an artificial imaginary addition may be added to the permittivity of the photonic crystal slab. Note that in contrast to the total Purcell factor, the integral for the external Purcell factor does not diverge.

In addition to the radiative decay rate Γ_r , there is also a nonradiative decay rate Γ_{nr} , which is attributed to non-electromagnetic recombination channels, i.e., which cannot be described by Maxwell's equations [63]. By definition, non-radiative decay occurs without emission of real photons and does not depend on the optical modes of the structure [63]. The total decay rate in the cavity is the sum of the radiative and nonradiative parts:

$$\Gamma_{\text{tot}}^{\text{cav}}(\omega, \vec{r}) = F_p^{\text{tot}}(\omega, \vec{r})\Gamma_r + \Gamma_{nr}. \quad (\text{C2})$$

In formula (C2), the values of Γ_r and Γ_{nr} depend only on the type of emitters and such properties of the host matrix

as temperature, chemical composition, presence of impurities and defects and so on. It should be noted that sometimes in the literature (for example, in the Refs. [64,65]) the nonradiative decay rate is also understood as the component of the total Purcell factor corresponding to the integration in formula (B5) below the light cone.

To characterize how efficiently the emitters can radiate in a given dielectric environment, one can use quantitative measures referred to as an internal quantum efficiency (IQE) and an external quantum efficiency (EQE) defined as

$$\text{IQE} = \frac{\Gamma_r}{\Gamma_r + \Gamma_{nr}}, \quad \text{EQE} = \frac{\Gamma_r F_p^{\text{ext}}}{\Gamma_r F_p^{\text{tot}} + \Gamma_{nr}}. \quad (\text{C3})$$

By this definition, the external quantum efficiency is a characteristic of both the host matrix and the resonator where the dipole is located, while the internal quantum efficiency is a characteristic only of the host matrix. At $\Gamma_{nr} \ll \Gamma_r$ [54], high values of EQE can be obtained when the external Purcell factor is not small compared to the total Purcell factor. In particular, in photonic crystal slabs at frequencies larger than the upper diffraction threshold, the total and external Purcell factors are equal to each other $F_p^{\text{tot}} = F_p^{\text{ext}}$, which at small Γ_{nr} leads to almost 100% external quantum efficiencies. In plasmonic nanoparticles the situation is different: they can provide very large spontaneous emission rates (much larger than those in photonic crystal slabs), but in order to attain high external quantum efficiencies, one has to choose the geometry of nanoparticles properly to ensure that the near-field modes are coupled to the far field [4–6]. The possibility of the latter is not guaranteed in plasmonic nanoparticles in contrast to photonic crystal slabs.

APPENDIX D: PURCELL FACTOR OF DIPOLES IN ONE-DIMENSIONAL AND TWO-DIMENSIONAL PHOTONIC CRYSTAL SLABS

An alternative way of considering the Purcell factor is based on the resonant approximation for the system. It means that in calculation of the Purcell factor at a given frequency, one should gather contributions from the resonances nearest to this frequency, neglecting the background (i.e., neglecting the contribution from other resonances). In practice, this procedure sometimes appears to be rather challenging because one should know everything about the nearest resonances, which is not always an easy task. From the other hand, expansion over the resonances enables simple analytical expressions of local densities of optical states, which could give us insight on general properties of the system. To demonstrate this, let us obtain analytical expressions of the local density of optical states containing dependence on the group velocity. It should be noted that the very fact of using the concept of a group velocity already implies that we are using a resonant approximation for our system. We start from the following formula for the local density of optical states:

$$\varrho(\vec{r}, \omega) = \frac{1}{(2\pi)^2} \sum_n \iint_{\text{FBZ}} d^2\vec{q} \delta[\omega - \omega_n(\vec{q})] |\vec{E}_n(\vec{r}, \vec{q})|^2, \quad (\text{D1})$$

where ω_n is the frequency of n th resonance, $\vec{q} = (k_x, k_y)$ is the in-plane wave vector of the resonance, $\vec{E}_n(\vec{r}, \vec{q})$ is the electric field of n th resonance at position \vec{r} and in-plane wave vector \vec{q} . Then,

$$\varrho(\vec{r}, \omega) = \frac{1}{(2\pi)^2} \sum_n \iint_{\text{FBZ}} d^2\vec{q} \delta[\omega - \omega_n(\vec{q})] |\vec{E}_n(\vec{r}, \vec{q})|^2 = \frac{1}{(2\pi)^2} \sum_n \iint \delta[\omega - \omega_n(\vec{q})] |\vec{E}_n(\vec{r}, \vec{q})|^2 \left| \frac{\partial(k_x, k_y)}{\partial(\omega_n, \Gamma_n)} \right| d\omega_n d\Gamma_n, \quad (\text{D2})$$

where Γ_n is the isofrequency contour of the n th mode. Taking into account that

$$\left| \frac{\partial(\omega_n, \Gamma_n)}{\partial(k_x, k_y)} \right| = \left| \det \begin{pmatrix} \frac{\partial\omega_n}{\partial k_x} & \frac{\partial\omega_n}{\partial k_y} \\ \frac{\partial\Gamma_n}{\partial k_x} & \frac{\partial\Gamma_n}{\partial k_y} \end{pmatrix} \right| = |(\mathbf{V}_n^{\text{gr}} \times \boldsymbol{\tau}_n)_z| = |\mathbf{V}_n^{\text{gr}}(\omega_n, \Gamma_n)|, \quad (\text{D3})$$

where $\boldsymbol{\tau}_n = \partial\Gamma_n/\partial\mathbf{q}$ is the unitary vector tangent to the isofrequency contour, we obtain finally:

$$\varrho(\vec{r}, \omega) = \frac{1}{(2\pi)^2} \sum_n \iint \delta[\omega - \omega_n(\vec{q})] |\vec{E}_n(\vec{r}, \vec{q})|^2 \left| \frac{\partial(k_x, k_y)}{\partial(\omega_n, \Gamma_n)} \right| d\omega_n d\Gamma_n = \frac{1}{(2\pi)^2} \sum_n \int \frac{|\vec{E}_n(\vec{r}, \omega, \Gamma_n)|^2}{|\mathbf{V}_n^{\text{gr}}(\omega, \Gamma_n)|} d\Gamma_n. \quad (\text{D4})$$

Despite the group velocity of the resonances at some points (ω_n, \vec{q}_n) equals to zero, the integral (D4) is not diverging, in general, even at resonant frequencies ω_n , due to the integration over the entire first Brillouin zone. In one-dimensional chains the situation is different, because the final formula for the local density of states contains summation over the resonances:

$$\varrho(\vec{r}, \omega, \vec{e}_d) = \frac{1}{2\pi} \sum_n \int d\vec{q} \delta[\omega - \omega_n(\vec{q})] |\vec{E}_n(\vec{r}, \vec{q})|^2 = \frac{1}{2\pi} \sum_n \frac{|\vec{E}_n(\vec{r}, q_n(\omega), \varphi)|^2}{\left| \frac{\partial\omega(q_n(\omega), \varphi)}{\partial\vec{q}} \right|} = \frac{1}{2\pi} \sum_n \frac{|\vec{E}_n(\vec{r}, q_n(\omega), \varphi)|^2}{|V_{\text{gr}}(\omega, q_n(\omega), \varphi)|}. \quad (\text{D5})$$

Since the group velocity vanishes at resonance frequencies on the edge of the first Brillouin zone, the local density of states in one-dimensional chains diverges. This situation is considered in Refs. [17,20]. We emphasize, that the formulas (D1)–(D5) applicable only to resonant systems, optical properties of which can be more or less conveniently described by considering a set of resonances. In contrast to this, formula (8) in our manuscript represents a rigorous

procedure for calculating the Purcell factor in any two-dimensional photonic crystal slab without point or line defects with arbitrary unit cell consisting of arbitrary number of layers. Therefore, despite the visual simplicity of formulas for the Purcell factor containing the group velocity (as well as other effective parameters), the use of them sometimes is not at all easier than evaluating the integral in expression (8).

-
- [1] C. Sauvan, J.-P. Hugonin, I. S. Maksymov, and P. Lalanne, *Phys. Rev. Lett.* **110**, 237401 (2013).
- [2] A. F. Koenderink, *Opt. Lett.* **35**, 4208 (2010).
- [3] S. V. Lobanov, T. Weiss, D. Dregely, H. Giessen, N. A. Gippius, and S. G. Tikhodeev, *Phys. Rev. B* **85**, 155137 (2012).
- [4] O. Pavelka, S. Dyakov, K. Kvakova, J. Vesely, P. Cigler, and J. Valenta, *Nanoscale* **15**, 3351 (2023).
- [5] O. Pavelka, S. Dyakov, J. Vesely, A. Fučíková, H. Sugimoto, M. Fujii, and J. Valenta, *Nanoscale* **13**, 5045 (2021).
- [6] G. M. Akselrod, C. Argyropoulos, T. B. Hoang, C. Ciraci, C. Fang, J. Huang, D. R. Smith, and M. H. Mikkelsen, *Nat. Photon.* **8**, 835 (2014).
- [7] K. L. Tsakmakidis, O. Hess, R. W. Boyd, and X. Zhang, *Science* **358**, eaan5196 (2017).
- [8] K. L. Tsakmakidis, R. W. Boyd, E. Yablonovitch, and X. Zhang, *Opt. Express* **24**, 17916 (2016).
- [9] A. N. Poddubny, P. A. Belov, P. Ginzburg, A. V. Zayats, and Y. S. Kivshar, *Phys. Rev. B* **86**, 035148 (2012).
- [10] I. Iorsh, A. Poddubny, A. Orlov, P. Belov, and Y. S. Kivshar, *Phys. Lett. A* **376**, 185 (2012).
- [11] J.-M. Gerard and B. Gayral, *J. Lightwave Technol.* **17**, 2089 (1999).
- [12] A. Barreda, L. Mercadé, M. Zapata-Herrera, J. Aizpurua, and A. Martínez, *Phys. Rev. Appl.* **18**, 044066 (2022).
- [13] M. K. Schmidt, R. Esteban, J. Sáenz, I. Suárez-Lacalle, S. Mackowski, and J. Aizpurua, *Opt. Express* **20**, 13636 (2012).
- [14] R. Savelev, S. Makarov, A. Krasnok, and P. Belov, *Opt. Spectrosc.* **119**, 551 (2015).
- [15] A. E. Krasnok, A. P. Slobozhanyuk, C. R. Simovski, S. A. Tretyakov, A. N. Poddubny, A. E. Miroshnichenko, Y. S. Kivshar, and P. A. Belov, *Sci. Rep.* **5**, 12956 (2015).
- [16] L. Van Hove, *Phys. Rev.* **89**, 1189 (1953).
- [17] A. Krasnok, S. Glybovski, M. Petrov, S. Makarov, R. Savelev, P. Belov, C. Simovski, and Y. Kivshar, *Appl. Phys. Lett.* **108**, 211105 (2016).
- [18] T. X. Hoang, S. T. Ha, Z. Pan, W. K. Phua, R. Paniagua-Domínguez, C. E. Png, H.-S. Chu, and A. I. Kuznetsov, *Nano Lett.* **20**, 5655 (2020).
- [19] A. Krasnok, S. Li, S. Lepeshov, R. Savelev, D. G. Baranov, and A. Alú, *Phys. Rev. Appl.* **9**, 014015 (2018).
- [20] D. F. Kornovan, R. S. Savelev, Y. Kivshar, and M. I. Petrov, *ACS Photonics* **8**, 3627 (2021).
- [21] S. A. Dyakov, M. V. Stepikhova, A. A. Bogdanov, A. V. Novikov, D. V. Yurasov, M. V. Shaleev, Z. F. Krasilnik, S. G. Tikhodeev, and N. A. Gippius, *Laser Photonics Rev.* **15**, 2000242 (2021).
- [22] M. Panmai, J. Xiang, S. Li, X. He, Y. Ren, M. Zeng, J. She, J. Li, and S. Lan, *Nat. Commun.* **13**, 2749 (2022).

- [23] S. Yuan, X. Qiu, C. Cui, L. Zhu, Y. Wang, Y. Li, J. Song, Q. Huang, and J. Xia, *ACS Nano* **11**, 10704 (2017).
- [24] A. Kodigala, T. Lepetit, Q. Gu, B. Bahari, Y. Fainman, and B. Kanté, *Nature (London)* **541**, 196 (2017).
- [25] S. T. Ha, Y. H. Fu, N. K. Emani, Z. Pan, R. M. Bakker, R. Paniagua-Domínguez, and A. I. Kuznetsov, *Nat. Nanotechnol.* **13**, 1042 (2018).
- [26] A. Barreda, C. Zou, A. Sinelnik, E. Menshikov, I. Sinev, T. Pertsch, and I. Staude, *Opt. Mater. Express* **12**, 3132 (2022).
- [27] A. V. Novikov, Z. V. Smagina, M. V. Stepikhova, V. A. Zinovyev, S. A. Rudin, S. A. Dyakov, E. E. Rodyakina, A. V. Nenashev, S. M. Sergeev, A. V. Peretokin *et al.*, *Nanomaterials* **11**, 909 (2021).
- [28] K. L. Koshelev, Z. F. Sadrieva, A. A. Shcherbakov, Y. S. Kivshar, and A. A. Bogdanov, *Phys. Usp.* **66**, 494 (2023).
- [29] A. V. Peretokin, M. V. Stepikhova, A. V. Novikov, S. A. Dyakov, A. F. Zinovieva, Zh. V. Smagina, D. A. Nasimov, E. E. Rodyakina, and V. A. Zinovyev, *Photonics Nanostruct.* **53**, 101093 (2023).
- [30] D. Yurasov, A. Yablonskiy, N. Baidakova, M. Shaleev, E. Rodyakina, S. Dyakov, and A. Novikov, *J. Phys. D* **55**, 075107 (2022).
- [31] M. V. Stepikhova, S. A. Dyakov, A. V. Peretokin, M. V. Shaleev, E. E. Rodyakina, and A. V. Novikov, *Nanomaterials* **12**, 2687 (2022).
- [32] A. V. Peretokin, D. V. Yurasov, M. V. Stepikhova, M. V. Shaleev, A. N. Yablonskiy, D. V. Shengurov, S. A. Dyakov, E. E. Rodyakina, Z. V. Smagina, and A. V. Novikov, *Nanomaterials* **13**, 1678 (2023).
- [33] F. Lemarchand, A. Sentenac, and H. Giovannini, *Opt. Lett.* **23**, 1149 (1998).
- [34] V. S. C. Manga Rao and S. Hughes, *Phys. Rev. B* **75**, 205437 (2007).
- [35] S. Noda, M. Fujita, and T. Asano, *Nat. Photon.* **1**, 449 (2007).
- [36] E. Nussbaum, N. Rotenberg, and S. Hughes, *Phys. Rev. A* **106**, 033514 (2022).
- [37] L. Sanchis, M. J. Cryan, J. Pozo, I. J. Craddock, and J. G. Rarity, *Phys. Rev. B* **76**, 045118 (2007).
- [38] M. Patterson, S. Hughes, D. Dalacu, and R. L. Williams, *Phys. Rev. B* **80**, 125307 (2009).
- [39] A. Taflove, A. Oskooi, and S. G. Johnson (eds.), *Advances in FDTD Computational Electrodynamics: Photonics and Nanotechnology* (Artech House, Washington, D.C., 2013).
- [40] A. Oskooi and S. G. Johnson, *arXiv:1301.5366*.
- [41] S. G. Tikhodeev, A. L. Yablonskii, E. A. Muljarov, N. A. Gippius, and T. Ishihara, *Phys. Rev. B* **66**, 045102 (2002).
- [42] M. Moharam, T. Gaylord, E. B. Grann, and D. A. Pommet, *J. Opt. Soc. Am. A* **12**, 1068 (1995).
- [43] H. Taniyama and M. Notomi, *J. Appl. Phys.* **103**, 083115 (2008).
- [44] S. A. Dyakov, N. A. Gippius, I. M. Fradkin, and S. G. Tikhodeev, *Phys. Rev. Appl.* **14**, 024090 (2020).
- [45] Y. Chen, Y. Zhang, and A. F. Koenderink, *Opt. Express* **25**, 21358 (2017).
- [46] F. Capolino, D. R. Jackson, D. R. Wilton, and L. B. Felsen, *IEEE Trans. Antennas Propag.* **55**, 1644 (2007).
- [47] L. Novotny and B. Hecht, *Principles of Nano-Optics* (Cambridge University Press, Cambridge, 2012).
- [48] N. A. Gippius, T. Weiss, S. G. Tikhodeev, and H. Giessen, *Opt. Express* **18**, 7569 (2010).
- [49] D. Gromyko, I. Fradkin, S. Dyakov, and N. Gippius, *Mater. Proc.* **4**, 34 (2020).
- [50] D. A. Gromyko, S. A. Dyakov, S. G. Tikhodeev, and N. A. Gippius, *Photonics Nanostruct.* **53**, 101109 (2023).
- [51] D. A. Gromyko, S. A. Dyakov, S. G. Tikhodeev, and N. A. Gippius, *Photonics Nanostruct.* **53**, 101110 (2023).
- [52] S. Miura, T. Nakamura, M. Fujii, M. Inui, and S. Hayashi, *Phys. Rev. B* **73**, 245333 (2006).
- [53] R. J. Walters, J. Kalkman, A. Polman, H. A. Atwater, and M. J. A. de Dood, *Phys. Rev. B* **73**, 132302 (2006).
- [54] J. Valenta, M. Greben, S. Dyakov, N. Gippius, D. Hiller, S. Gutsch, and M. Zacharias, *Sci. Rep.* **9**, 11214 (2019).
- [55] According to the formalism of the Fourier modal method, we solve the Maxwell's equations in the photonic crystal slab by expanding the electromagnetic field into the N_g Fourier harmonics, and connect the solutions in each layer by taking into account the continuity conditions of the field components. In the result, we calculate the scattering matrix with dimensionality $4N_g \times 4N_g$, which contains the full optical information about the system. The more harmonics we use, the more precise result we obtain, but the longer time it takes to calculate the scattering matrix.
- [56] See Supplemental Material at <http://link.aps.org/supplemental/10.1103/PhysRevB.108.155416> for (1) the dependence of the external and total Purcell factors of vertical and horizontal dipoles inside a homogeneous silicon slab on the artificially added imaginary part of permittivity; (2) the photon energy and in-plane wave-vector dependence of the near-field emissivity of the direct and inverse photonic crystal slabs calculated for points A, B, and C of the photonic crystal lattice unit cell and x , y , z dipoles; (3) the spectra of the total Purcell factor and its partial contributions from different energy dissipation channels calculated for the direct and inverse photonic crystal slab in points A, B, and C of the photonic crystal lattice unit cell and x , y , z dipoles; (4) near-field and far-field emissivities in the first Brillouin zone, calculated for the direct and inverse photonic crystal slabs for points A, B, C, and x , y , z dipoles.
- [57] D. M. Whittaker and I. S. Culshaw, *Phys. Rev. B* **60**, 2610 (1999).
- [58] D. Whittaker, *Opt. Lett.* **25**, 779 (2000).
- [59] I. M. Fradkin, S. A. Dyakov, and N. A. Gippius, *Phys. Rev. B* **99**, 075310 (2019).
- [60] I. M. Fradkin, S. A. Dyakov, and N. A. Gippius, *Phys. Rev. B* **102**, 045432 (2020).
- [61] T. Weiss, N. a. Gippius, S. G. Tikhodeev, G. Granet, and H. Giessen, *J. Opt. A* **11**, 114019 (2009).
- [62] L. Li, *J. Opt. Soc. Am. A* **14**, 2758 (1997).
- [63] G. W. Ford and W. Weber, *Phys. Rep.* **113**, 195 (1984).
- [64] W. Barnes, *J. Mod. Opt.* **45**, 661 (1998).
- [65] S. Khatua, P. M. Paulo, H. Yuan, A. Gupta, P. Zijlstra, and M. Orrit, *ACS Nano* **8**, 4440 (2014).